Personalized Medicine and Imaging

Tumor-Specific Uptake of Fluorescent Bevacizumab–IRDye800CW Microdosing in Patients with Primary Breast Cancer: A Phase I Feasibility Study 🔓

Laetitia E. Lamberts[1], Maximillian Koch[2], Johannes S. de Jong[3], Arthur L.L. Adams[4], Jürgen Glatz[2], Mariëtte E.G. Kranendonk[3], Anton G.T. Terwisscha van Scheltinga[1,5], Liesbeth Jansen[6], Jakob de Vries[6], Marjolijn N. Lub-de Hooge[5], Carolien P. Schröder[1], Annelies Jorritsma-Smit[5], Matthijs D. Linssen[5], Esther de Boer[6], Bert van der Vegt[7], Wouter B. Nagengast[8], Sjoerd G. Elias[9], Sabrina Oliveira[10], Arjen J. Witkamp[11], Willem P.Th.M. Mali[4], Elsken Van der Wall[12], Paul J. van Diest[3], Elisabeth G.E. de Vries[1], Vasilis Ntziachristos[2], and Gooitzen M. van Dam[6,13,14]

Abstract

Purpose: To provide proof of principle of safety, breast tumor–specific uptake, and positive tumor margin assessment of the systemically administered near-infrared fluorescent tracer bevacizumab–IRDye800CW targeting VEGF-A in patients with breast cancer.

Experimental Design: Twenty patients with primary invasive breast cancer eligible for primary surgery received 4.5 mg bevacizumab–IRDye800CW as intravenous bolus injection. Safety aspects were assessed as well as tracer uptake and tumor delineation during surgery and *ex vivo* in surgical specimens using an optical imaging system. *Ex vivo* multiplexed histopathology analyses were performed for evaluation of biodistribution of tracer uptake and coregistration of tumor tissue and healthy tissue.

Results: None of the patients experienced adverse events. Tracer levels in primary tumor tissue were higher compared with those in the tumor margin ($P < 0.05$) and healthy tissue ($P < 0.0001$). VEGF-A tumor levels also correlated with tracer levels ($r = 0.63$, $P < 0.0002$). All but one tumor showed specific tracer uptake. Two of 20 surgically excised lumps contained microscopic positive margins detected *ex vivo* by fluorescent macro- and microscopy and confirmed at the cellular level.

Conclusions: Our study shows that systemic administration of the bevacizumab–IRDye800CW tracer is safe for breast cancer guidance and confirms tumor and tumor margin uptake as evaluated by a systematic validation methodology. The findings are a step toward a phase II dose-finding study aimed at *in vivo* margin assessment and point to a novel drug assessment tool that provides a detailed picture of drug distribution in the tumor tissue. *Clin Cancer Res; 23(11); 2730–41. ©2016 AACR.*

Introduction

Breast cancer is the second most common cancer, with 522,000 deaths globally in 2012 and a rising incidence (1). Surgery is one of the three cornerstones of primary invasive breast cancer treatment, the other two being radiotherapy and systemic therapy. Tumor-free surgical margins are critical in breast-conserving sur-

gery (BCS), as local recurrence rates increase with positive resection margins (2–5). Therefore, patients with positive resection margins are often reoperated, causing higher surgical risks, poorer cosmetic results, psychologic and physical burden, and higher health care costs. Currently, preoperative imaging and tactile information are used during breast surgery to determine the size,

[1]Department of Medical Oncology, University Medical Center Groningen, University of Groningen, Groningen, the Netherlands. [2]Technische Universität München & Helmholtz Zentrum, München, Germany. [3]Department of Pathology, University Medical Center Utrecht, Utrecht University, Utrecht, the Netherlands. [4]Department of Radiology, University Medical Center Utrecht, Utrecht University, Utrecht, the Netherlands. [5]Hospital and Clinical Pharmacy, University Medical Center Groningen, University of Groningen, Groningen, the Netherlands. [6]Department of Surgery, University Medical Center Groningen, University of Groningen, Groningen, the Netherlands. [7]Department of Pathology, University Medical Center Groningen, University of Groningen, Groningen, the Netherlands. [8]Department of Gastroenterology, University Medical Center Groningen, University of Groningen, Groningen, the Netherlands. [9]Julius Center for Health Sciences and Primary Care, University Medical Center Utrecht, Utrecht University, Utrecht, the Netherlands. [10]Division of Cell Biology of the Department of Biology, University Medical Center Utrecht, Utrecht University, Utrecht, the Netherlands. [11]Department of Surgery, University Medical Center Utrecht,

Utrecht University, Utrecht, the Netherlands. [12]Department of Medical Oncology, University Medical Center Utrecht, Utrecht University, Utrecht, the Netherlands. [13]Department of Nuclear Medicine and Molecular Imaging, University Medical Center Groningen, University of Groningen, Groningen, the Netherlands. [14]Department of Intensive Care, University Medical Center Groningen, University of Groningen, Groningen, the Netherlands.

Corresponding Author: Gooitzen M. van Dam, University Medical Center Groningen, University of Groningen, Hanzeplein 1, Groningen 9700 RB, the Netherlands. Phone: 315-0361-2283; Fax: 315-0361-4873; E-mail: g.m.van.dam@umcg.nl

AACR

Translational Relevance

Tumor-free surgical margins are critical in breast-conserving surgery, as local recurrence rates increase with positive margins. Molecular imaging is a promising strategy for visualizing and quantifying tumor-specific molecular characteristics and potentially improves breast cancer care in terms of detection, characterization, and (non-)surgical treatment strategies. A potential target for molecular imaging is VEGF-A, involved in tumor angiogenesis. Our study shows that systemic administration of the fluorescent bevacizumab–IRDye800CW tracer is safe in *ex vivo* breast cancer guidance and confirms (tumor-) margin uptake providing a novel framework for systematic evaluation and validation of fluorescent tracers in image-guided surgery and drug development. As neoangiogenesis is a universal tumor marker, other tumor types like colorectal and esophageal cancer might benefit from fluorescence-guided molecular endoscopy using bevacizumab–IRDye800CW. This approach is of interest for surgical guidance, but also for diagnostic purposes, drug development, and treatment monitoring.

localization, and extent of the area that has to be removed. However, the efficacy of this approach is poor, with positive margin rates of 20% to 40% being reported worldwide (6).

Molecular imaging is a promising strategy to improve this efficacy; it can be used to visualize and quantify tumor-specific molecular characteristics and could potentially improve breast cancer care in terms of detection, characterization, and surgical and nonsurgical management strategies. A potential target for molecular imaging in breast cancer is VEGF-A, a soluble dimeric glycoprotein that is involved in tumor angiogenesis (7, 8). VEGF-A is frequently overexpressed in breast cancers with an expression rate of approximately 73% compared with normal breast tissue (9). It can therefore serve as a more generic tracer target (10, 11) without preselection of patients compared with other potential targets, such as HER2, which is overexpressed in only 10% to 20% of primary breast cancers (12–14).

The registered humanized mAb bevacizumab not only neutralizes all VEGF-A isoforms but can also be used as a radiolabeled imaging agent in combination with single photon emission CT (SPECT) and PET (15). Successful and specific imaging has been performed in patients with melanoma, renal cell cancer, neuroendocrine tumors, and breast cancer using [111]In- and [89]Zr-radiolabeled bevacizumab (11, 15–19). In these studies, a systemic total microdose of 4.5 mg labeled bevacizumab, that is, ≤30 nmol adhering to the definition of microdosing for proteins according to FDA/EMEA guidelines (20) and as described separately for proteins by Kummar and colleagues (21), was used, which is subtherapeutic compared with the therapeutic dose of 5 to 15 mg/kg bodyweight (22–24). In a recent PET imaging study with [89]Zr-bevacizumab in 23 patients with primary breast cancer, 25 of 26 tumors (96%) were visualized by PET 4 days after [89]Zr-bevacizumab tracer injection with tumor-to-normal tissue ratios of 1.4:10.3 (19). These results prompted us to design an optical imaging study based on the microdosing concept of using a therapeutic antibody as targeting moiety in patients undergoing breast cancer surgery.

Recently, optical fluorescence imaging has become suitable for clinical translation due to its favorable characteristics, such as absence of ionizing radiation, inherently low-cost technology, and its possibilities for real-time, intra-, and postoperative imaging. Two phase I feasibility studies in, respectively, patients with colorectal cancer imaged with a chimeric fluorescein-conjugated carcinoembryonic antigen (CEA)–targeted antibody (25) and patients with ovarian cancer using folate-fluorescein isothiocyanate (FITC, light emission at 400–650 nm) targeting the folate receptor-α demonstrated the great potential of optical imaging during surgery using a clinical prototype camera (26). However, clinical implementation studies have been obstructed by characteristics such as the limited penetration depth of fluorescent dyes such as fluorescein with emission in the visible light spectrum, the negative effects of optical properties, such as absorption, scattering, and the autofluorescence of tissue in the visible spectrum. To reduce background fluorescence and autofluorescence and increase tissue penetration, near-infrared fluorescent (NIRF) dyes must be used that have excitation wavelengths between 700 and 900 nm (27). More recently, Burggraaf and colleagues demonstrated c-met–targeted endoscopy fluorescence imaging in humans using a fluorescent dye of 650 nm (28), whereas Rosenthal and colleagues have demonstrated the feasibility of using the therapeutic mAb cetuximab targeting EGFR as the targeting moiety of an NIRF tracer in patients with head and neck cancer (29). In addition, the clinical application of a protease-activatable tracer has been reported in patients with soft tissue sarcoma and breast cancer (30).

Using bevacizumab conjugated to the NIRF dye IRDye800CW (peak absorption 778 nm, peak emission 795 nm), we decided to determine whether this approach could be used for intraoperative guidance in breast cancer surgery, combined with a novel systematic analytic methodology for *ex vivo* evaluation of tumor specificity and microdistribution. Bevacizumab–IRDye800CW showed high levels of accumulation in human breast cancer–bearing mouse tumors (31), leading to good manufacturing practice (GMP) production of clinical grade bevacizumab–IRDye800CW for human use (32). In conjunction with the progress in the development of NIR intraoperative optical imaging systems for clinical applications, we initiated this first-in-human clinical study of clinical grade bevacizumab–IRDye800CW in patients with breast cancer.

The primary aims of our feasibility study were to provide proof of principle of safety, tumor-specific uptake, and tumor margin assessment of the intravenously administered NIRF microdose tracer bevacizumab–IRDye800CW, targeting VEGF-A in patients with primary invasive breast cancer, as validated *ex vivo* by multiplex advanced pathology imaging (MAPI).

Materials and Methods

Trial design

The study was a two-center, first-in-human, two-stage, non-randomized, nonblinded, prospective, feasibility study in patients with histologically proven breast cancer scheduled for surgery (registered at www.ClinicalTrials.gov, identifier NCT01508572). Primary endpoints were the occurrence of serious adverse events (adverse events were classified according to the NCI Common Terminology Criteria for Adverse Events, Version 4.0) and accumulation of bevacizumab–IRDye800CW in breast cancer tissue and surrounding tissue in surgical specimen by fluorescence

macroscopy and microscopy. Additional information is provided in Supplementary Materials and Methods, section "trial design." The Institutional Review Board (IRB) of the University Medical Center Groningen (UMCG; Groningen, the Netherlands) approved the study, with local agreement of the University Medical Center Utrecht (UMCU; Utrecht, the Netherlands). All patients gave written informed consent.

Bevacizumab–IRDye800CW preparation and injection

Clinical grade bevacizumab–IRDye800CW was produced in the GMP facility of the UMCG by labeling bevacizumab (Roche AG) and IRDye800CW-NHS (LI-COR Biosciences Inc.) under regulated conditions as described previously (31). The molecular weight of the protein bevacizumab is 149 kDa. The fluorescent dye has a molecular weight of 1.166 kDa. With an average conjugation ratio of 1:4 protein:IRDye800CW, the total molecular weight is 1.537 kDa. This means for our 4.5 mg tracer dose bevacizumab–IRDye800CW, which translates into 26 nmol of bevacizumab-IRDye800CW, adhering to the FDA/EMA regulations of micro-dosing for proteins and according to the Task Force on Methodology for the Development of Innovative Cancer Therapies (20, 21). Additional information is provided in the Supplementary Materials and Methods, section "bevacizumab–IRDye800CW preparation and injection."

Surgical procedures and specimen handling

Patients underwent mastectomy or lumpectomy with or without a sentinel lymph node (SLN) procedure or axillary lymph node dissection, according to standard-of-care procedures and guidelines applicable for breast cancer in the Netherlands (33). During the study period, the positive margin rate for the UMCG was 7.8%, and for the UMCU, it was 5.2%.

In short, the SLN procedure was carried out by peritumoral injection of technetium-99m nanocolloid, followed by lymph scintigraphy after 2 to 3 hours. During surgery, a hand-held gamma counter was used to detect the radioactive signal from the SLN. After the first patient, the protocol was amended to omit patent blue V (Guerbet Asia Pacific) for visualization of the SLN if possible, as this dye interfered with the fluorescent signal after systemic microdosing 4.5 mg bevacizumab–IRDye800CW in this patient during surgery.

During surgery, images were recorded at several predefined time points during removal of the tumor and SLN with the optical imaging system (for further details see Supplementary Material, section "optical imaging system"). A baseline image was recorded before incision of the breast, followed by imaging of the tumor, before removal of the tumor (lumpectomy or mastectomy) at a distance suitable for the fluorescent signal (on average, 10–15 cm above the operating field), but not interfering with the sterile field of surgery. Using the optical imaging system prior to incision at the maximum field of view, the presence of a fluorescence signal was determined either in the tumor or axillary region. Identified (S)LNs were imaged prior to excision. After removal of the tumor and SLN, the surgical field was inspected again for remaining fluorescent signals. The surgical approach could only be adapted to the intraoperative findings if this would not have a negative impact on the actual outcome of the surgical procedure, as judged by the attending breast cancer surgeon (L. Jansen, J. de Vries, and A.J. Witkamp) in terms of cosmetic outcome and impaired wound healing. Subsequently, excised tumor tissue and SLN(s) were imaged ex vivo off-table directly after removal. Next, the surgical specimen was processed by the pathologist for ex vivo analysis of

tumor samples according to standard procedures and including imaging of the specimen as described in the subsection "ex vivo analyses of tumor samples." For all tumors besides determination of size, extent, and presence of in situ carcinoma, expression of estrogen receptor (ER), progesterone receptor (PR), and HER2 histologic grade and type according to the modified Bloom and Richardson and WHO guidelines was also performed according to standard clinical practice.

Follow-up

Adverse events occurring through approximately 2 weeks after surgery were recorded as spontaneously reported by patients or at an outpatient visit.

Ex vivo analyses of tumor samples

The following subsections are provided in the Supplementary Materials and Methods, section "ex vivo analyses of tumor samples": (i) imaging fresh surgical specimen; (ii) imaging FFPE blocks and slides; (iii) bevacizumab–IRDye800CW (34) and VEGF-A quantification; (iv) IHC; (v) fluorescence microscopy; and (vi) MAPI methodology.

Statistical analysis

Details on statistical analysis and power calculations for detecting potentially clinically relevant bevacizumab–IRDye800CW breast accumulation in patient with primary breast cancer are provided in Supplemental Material, section "statistical analysis."

Results

Patient characteristics

Between March 2012 and August 2014, we enrolled 20 patients with breast cancer (including one male patient) in the study. Patient and tumor characteristics are summarized in Table 1. Most patients had an invasive ductal carcinoma ($n = 17$, 85%), and three had an invasive ductulolobular carcinoma. Tumor size determined by pathology ranged from 6 to 38 mm (median 20 mm) in diameter. Histologic analyses after surgery of the tumor showed Bloom–Richardson–Elston histology grade 1 in six tumors, grade 2 in 10 tumors, and grade 3 in four tumors. ER status was positive in 18 patients (90%), PR status was positive in 14 patients (70%), and HER2 expression scores were negative in 13 patients (65%), 1+ in five patients, 2+ in one patient, and 3+ in one patient. In three patients, all the excised tissue was required for standard histologic examination due to the small tumor sizes of 6 mm. Two patients (10%) undergoing BCS through a lumpectomy had a positive resection margin on standard histopathologic examination, and 18 none.

No adverse events related to the tracer injection occurred in any of the patients, nor aberrations in hematology or blood chemistry levels. Tumor recurrence occurred in none of the patients during follow-up after surgery.

Intraoperative Imaging

Specimens from two patients were identified with a microscopic irradical resection (i.e., the positive margin) upon histopathologic analysis (Fig. 1; Supplementary Fig. S1). In both patients, a fluorescent signal was detectable at the positive resection margin of the excised lump (Fig. 1A–C), although not visible during surgery, but clearly visible on the back table during the surgical

Table 1. Patient demographic and pathologic characteristics

Characteristics	N (%)	Median (range)
Gender, female	19 (95)	
Surgery		
Lumpectomy	11 (55)	
Mastectomy	9 (45)	
Side tumor		
Right	8 (40)	
Left	12 (60)	
Age (y)		65 (46–81)
Tumor size (mm)		
Conventional imaging before surgery		
Ultrasound		15 (4–40)
MRI ($n = 1$)		28
Pathology		20 (6–38)
Histology		
Ductal carcinoma	17 (85)	
Ductulolobular carcinoma	3 (15)	
Bloom–Richardson–Elston grade		
Grade 1	6 (30)	
Grade 2	10 (50)	
Grade 3	4 (20)	
Receptor status		
ER$^+$	18 (90)	
PR$^+$	14 (70)	
HER2 (IHC 3+ or 2+ with FISH positive)	1 (5)	
Ductal carcinoma in situ component ($n = 15$)		
Grade 1	2 (13.3)	
Grade 2	10 (66.7)	
Grade 3	2 (13.3)	
Intracystic papillary carcinoma	1 (6.7)	
Pathologic tumor stage		
T1a	0 (0)	
T1b	4 (20)	
T1c	6 (30)	
T2	10 (50)	
Pathologic nodal stage		
N0	13 (65)	
N1	7 (35)	
Positive surgical margin	2 (10)	

NOTE: Tumor grade according to the Bloom–Richardson–Elston system (grade 1, 2, or 3).

procedure and after bread-loaf slicing (Fig. 1D–F). The paraffin block (Fig. 1G - 1I) also showed a clear positive signal at the tumor site. Hematoxylin and eosin stain (H&E, Fig. 1J) findings were corroborated by fluorescence flatbed scanning (Fig. 1K) and overlay image (Fig. 1L). This confirmed the presence of bevacizumab–IRDye800CW in the tumor area and the designated positive margin in both patients. Supplementary Figure S1 shows the surgical specimen from the second patient with a positive margin, visualized with our standard operating procedure for *ex vivo* processing. Fluorescence imaging shows strong signals at the vicinity of the margin in the bread-loaf slices (Supplementary Fig. S1A), which was confirmed by NIR optical imaging of paraffin blocks (Supplementary Fig. S1B, tumor is demarcated by red segmentation), H&E staining (Supplementary Fig. S1C), and fluorescence flatbed scanning (Supplementary Fig. S1D and S1E). With one exception, we detected a fluorescent signal in the excised specimens of all patients who were injected with bevacizumab–IRDye800CW. In the first patient, a male with breast cancer, in whom we could not detect a fluorescent signal *ex vivo*, a fluorescent signal prior to incision in the breast was visible but disappeared upon injection of patent blue (patent blue V sodium guerbet 2.5% solution for injection, 1 mL peritumoral injection) as part of the SLN procedure. For the remaining 19 patients, patent

blue was omitted within the SLN protocol and accordingly approved by the local IRB. It was concluded that the disappearance of the NIR fluorescence originating from the systemic injection of a microdose of bevacizumab–IRDye800CW in the tissue specimen was due to complete absorbance by the abundant peritumoral injection of patent blue and therefore subsequently omitted. Excised specimens were imaged by flatbed scanning of the paraffin blocks. Patients who were not injected with bevacizumab–IRDye800CW (negative controls) did not show fluorescent signals above background levels in tumor areas (Supplementary Fig. S2). In one patient, the skin was very fluorescent, and in one patient, a fibroadenoma adjacent to the tumor showed a clear fluorescent signal. In all patients, a standard operating procedure for *ex vivo* processing of surgical specimen was applied (Fig. 2).

Bevacizumab–IRDye800CW blood and tissue concentrations

The whole-blood concentrations of bevacizumab–IRDye800CW decreased during 14 days after injection (Fig. 3A). The bevacizumab–IRDye800CW concentration in tumor tissue was higher compared with the margin ($P < 0.05$) or surrounding noncancerous tissue ($P < 0.0001$; Fig. 3B). VEGF-A levels differed between tumor and surrounding tissue ($P < 0.001$) and between margin and surrounding tissue ($P < 0.05$), but not between tumor and margin (not significant; Fig. 3C). Bevacizumab–IRDye800CW and VEGF-A concentrations by ELISA correlated in the tumor area ($r = 0.63$, $P = 0.0002$; Fig. 3D), but not significantly at the margin or surrounding noncancerous tissue (Fig. 3D–F). Additional SDS-PAGE analysis of tumor lysates of three patients confirmed the intactness of the bevacizumab–IRDye800CW tracer within the tumor.

Fluorescence imaging and tumor margins

To compare macroscopic fluorescence imaging with tumor margins, two methods were used: tumor area assessment by defining four tumor margin zones distant from the tumor and by segmentation (Fig. 4). After flatbed scanning (Fig. 4A) and H&E staining of the paraffin block (Fig. 4D), four margin zones of 5×20 mm were defined (tumor area, 0.5, 1.0, and 1.5 cm) and scanned (Fig. 4B), after which the mean fluorescence intensity (MFI) was determined (Fig. 4C). The MFI of the tumor area differed from the other three tumor margin zones (tumor vs. 0.5 cm, tumor vs. 1.0 cm, tumor vs. 1.5 cm, all $P < 0.0001$).

Similarly, segmentation for separating tumor, stroma, and fat was performed on the excised specimen after H&E staining (Fig. 4E–G). Next, the segmented areas were superimposed on the fluorescence flatbed scans (Fig. 4E), and the MFI was calculated (Fig. 4H). Tumor-segmented areas had a higher MFI compared with stroma ($P < 0.0001$) and fat ($P < 0.0001$), which also translated into a significant difference in target-to-background ratios for tumor/stroma versus tumor/fat ($P < 0.001$; Supplementary Fig. S2). In two patients with a positive margin, the margin was fluorescent, whereas in the remaining 18 patients with a negative margin, there was also no fluorescence in the resection margin. In 90% of all patients, there was adjacent/complete overlap of bevacizumab–IRDye800CW and VEGF-A immunohistochemical staining and in 10% no overlap (Fig. 5).

MAPI

For a more detailed analysis of the distribution of bevacizumab–IRDye800CW in tumor tissue, a standardized operating procedure for macro- and microscopic mapping was performed
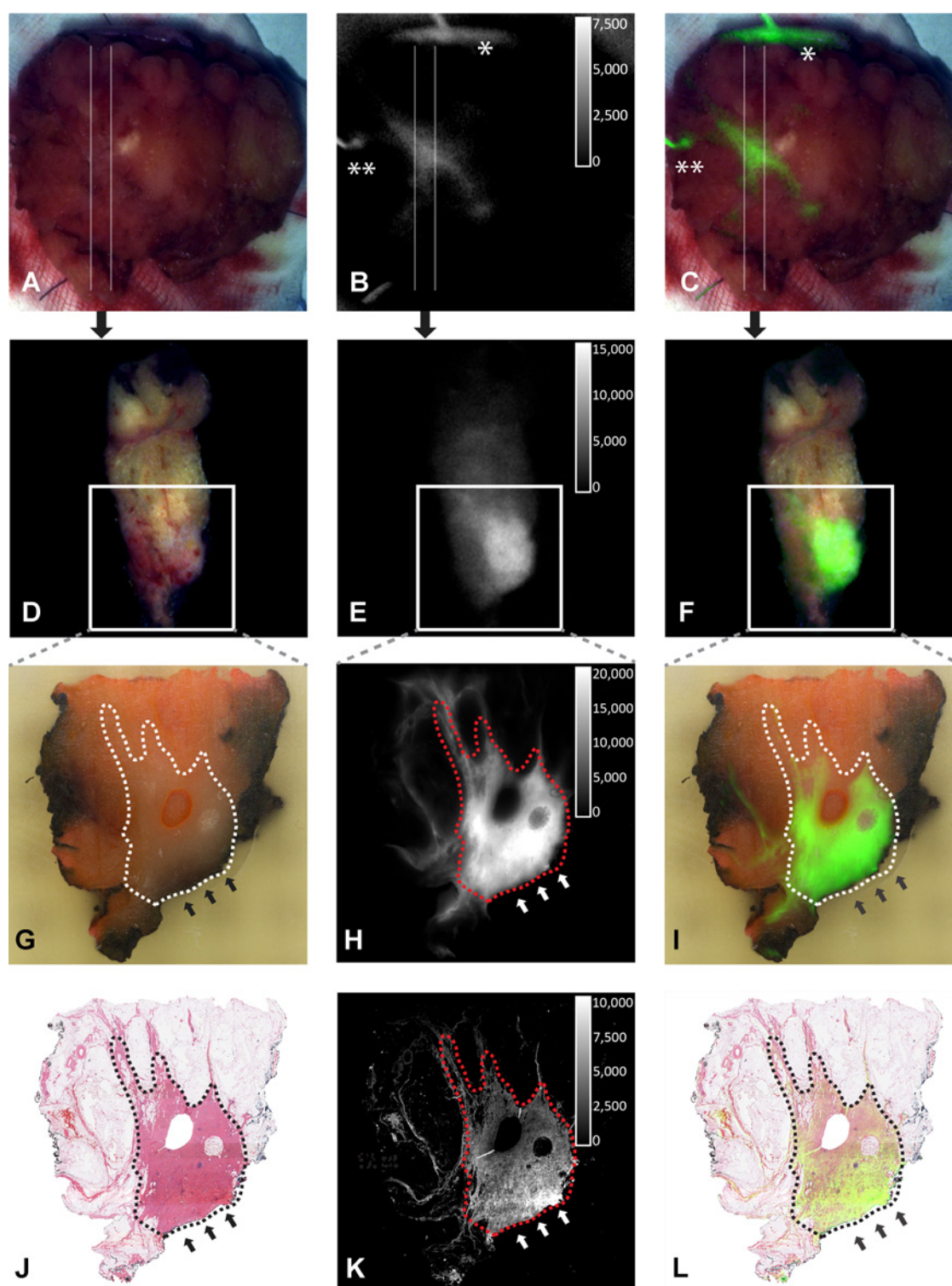
Figure 1.
Optical imaging of positive tumor margin. **A–C,** In one of the two patients (see also Supplementary Fig. S1) with a positive margin (tumor characteristics: lobular carcinoma, diameter 2.3 cm, Bloom–Richardson–Elston grade 1, mitotic activity index 2, estrogen receptor positive, progesterone receptor negative, HER2 negative), the bevacizumab–IRDye800CW tracer in the positive margin (black and white arrows) could be detected *ex vivo* by optical imaging of the excised lump (**A**, white-light; **B**, fluorescence; **C**, overlay with pseudocolor). **D–I,** Bread-loaf slicing (**D–F**) and the paraffin block (**G–I**) is shown for the corresponding fluorescent signal. **J–L,** H&E stain (**J**), fluorescence flatbed scanning (**K**), and image overlay of **J** and **K** (**L**) is shown for the 4-μm slide (*, skin with suture in place; **, satellite tumor foci; red/white/black dashed line, tumor outline; white/black arrow, positive tumor margin).
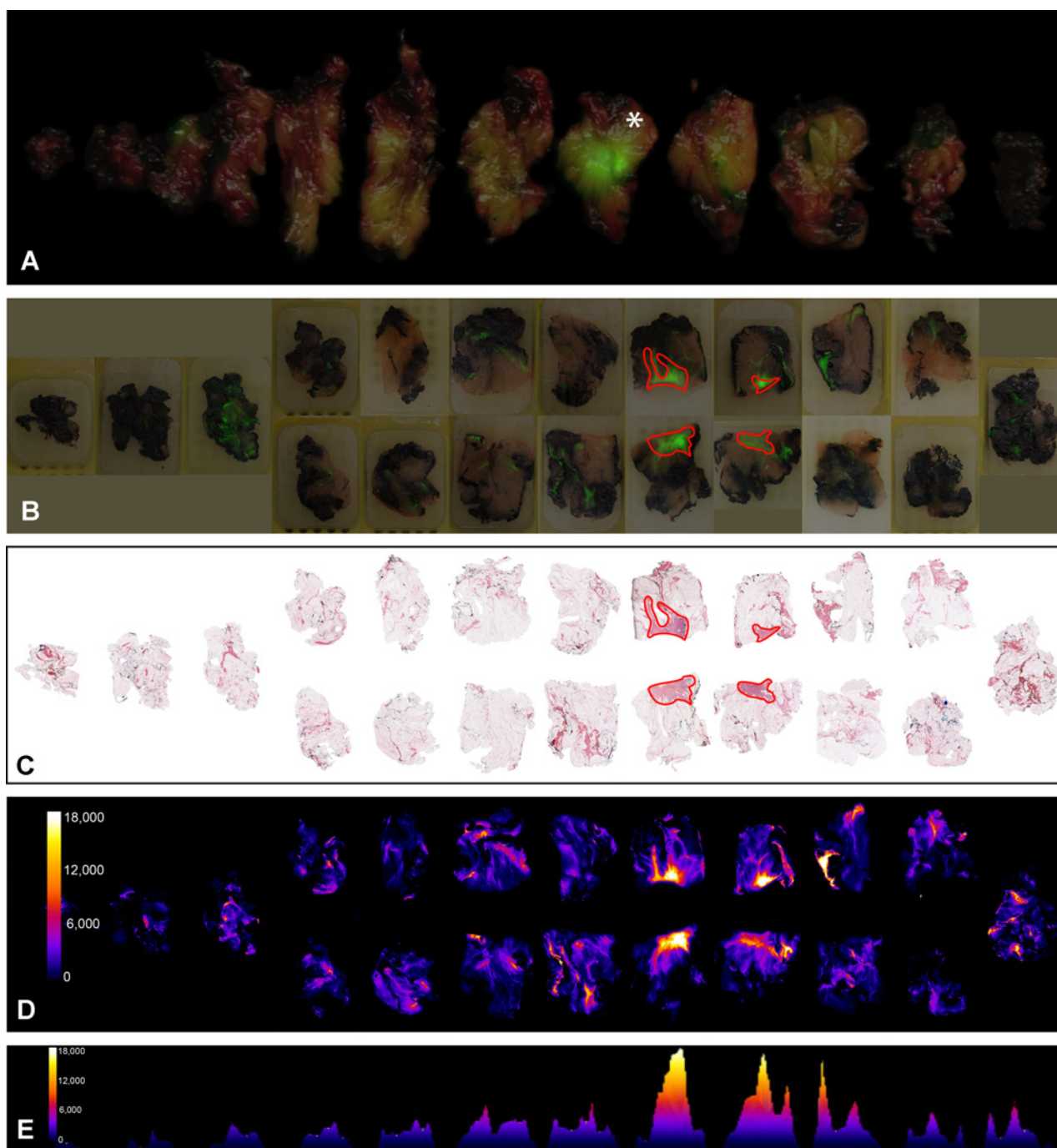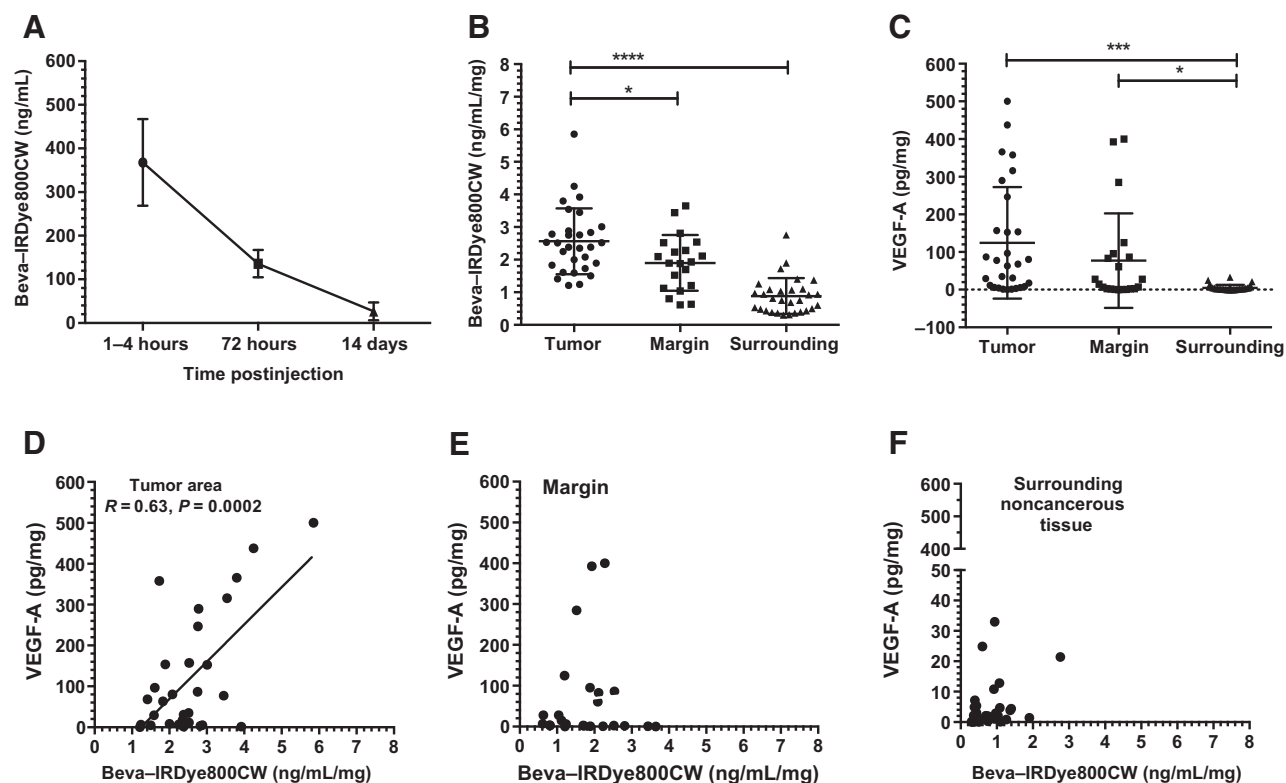
Figure 2.
Standard operating procedure for *ex vivo* processing of surgical specimen. Upon excision during surgery, the entire fresh specimen was cut into bread-loaf slices and imaged by the optical imaging system in overlay images of white light and fluorescence mode (**A,** Fluorescence, green pseudocolor; asterisk, tumor). Next, tissue was embedded into paraffin blocks and overlay images of white light and fluorescence were taken (**B,** Red, tumor border; green, pseudocolor for fluorescence). **C,** H&E staining is shown of slides from the same paraffin blocks (red, tumor localization) for colocalization purposes with the fluorescence images. Prior to H&E staining, the paraffin blocks were scanned on a flatbed scanner (**D,** Depicted in MFI), and also depicted as a Manhattan intensity graph in **E**.

at a macroscopic level as depicted in Fig. 2 and at the cellular level in Supplementary Figs. S3–S5.

H&E staining of 4-µm tissue slides (Supplementary Fig. S3A and S3B) was compared with fluorescence scanning (Supplementary Fig. S3C and S3D). In a superimposed image, both modalities were compared on a macroscopic and microscopic level (Supplementary Fig. S3E and S3F). Fluorescence signal was clearly identified in a tumor sprout surrounded by blood vessels and

Lamberts et al.

Figure 3.

Ex vivo quantification of bevacizumab–IRDye800CW and VEGF-A in whole blood and tissue. Blood concentration levels (mean ± SD) of bevacizumab–IRDye800CW (ng/mL) decreased 14 days after injection of the tracer (**A**). In tumor tissue biopsies, there was a higher concentration of bevacizumab–IRDye800CW (ng/mL/mg of weight biopsy tissue) compared with the tumor margin (*, $P < 0.05$) and surrounding (noncancerous) tissue (****, $P < 0.0001$; **B**). VEGF-A (pg/mg) concentrations differed significantly between tumor versus surrounding tissue (***, $P < 0.001$) and margin versus surrounding tissue (*, $P < 0.05$), but not between tumor area and margin (not significant; **C**). **D–F**, Bevacizumab–IRDye800CW and VEGF-A correlated in the tumor area ($r = 0.63$; $P = 0.0002$; **D**), which was not apparent at the margin (**E**), or in surrounding noncancerous tissue (**F**).

collagen-rich stroma (rectangle, Supplementary Fig. S3B, S3D, and S3F). NIR fluorescence microscopy compared with colocalization of H&E staining for tumor (margin) specificity clearly indicated tumor-specific staining of bevacizumab–IRDye800CW (Supplementary Fig. S3G and S3H).

For qualitative colocalization of bevacizumab–IRDye800CW with other biomarkers, such as VEGF-A expression, CD34 staining for microvessel density, and presence of collagen, MAPI was used (Supplemental Movie S1). Fluorescent bevacizumab–IRDye800CW scans were pseudocolored green, whereas hematoxylin-DAB/VEGF-A staining color intensities were color deconvoluted into pseudocolor red and superimposed with the pseudocolor green bevacizumab–IRDye800CW scans.

Supplementary Figure S4 shows the colocalization of bevacizumab–IRDye800CW, H&E, VEGF-A, collagen, and CD34 in breast cancer and a satellite lesion. A clear colocalization of fluorescence intensities as determined by fluorescence imaging (Supplementary Fig. S4A–S4D) is present within the tumor area (dotted lines). This was confirmed with H&E staining (Supplementary Fig. S4E), segmentation (Supplementary Fig. S4F), pseudocolor green bevacizumab–IRDye800CW flatbed scan (Supplementary Fig. S4G), and superimposed H&E with pseudocolor green (Supplementary Fig. S4H). Furthermore, colocalization of fluorescence and VEGF-A staining (Supplementary Fig. S4I),

collagen (Supplementary Fig. S4M), and CD34 (Supplementary Fig. S4Q) could be visualized as such. Additional data are provided for colocalization in ductal carcinoma *in situ* in Supplementary Fig. S5.

In 18 of 20 patients, lymph nodes were excised. Only three patients had a tumor-positive SLN, and 13 patients had a negative SLN. Two additional patients had lymph nodes with macrometastases: one of them had clinical suspicious macrometastatic lymph nodes, confirmed by ultrasound-guided biopsy and axillary lymph node dissection. Only in this patient we could even clearly identify fluorescence activity intraoperatively within the lymph node dissection specimen *in situ*, confirmed by *ex vivo* fluorescence and histopathologic analysis (Supplementary Fig. S6). There was no difference in VEGF-A immunohistochemical staining between tumor-positive lymph nodes and negative lymph nodes ($n = 104$ lymph node tissue blocks). Colocalization of NIR fluorescence showed mainly fluorescence surrounding the tumor cells within a lymph node (Supplementary Fig. S6), whereas in a tumor-negative lymph node, it was mainly centrally located in the lymph node (Supplementary Fig. S7).

Discussion

In this first-in-human study using an NIRF antibody-based tracer in a microdose regimen, administration of bevacizumab–
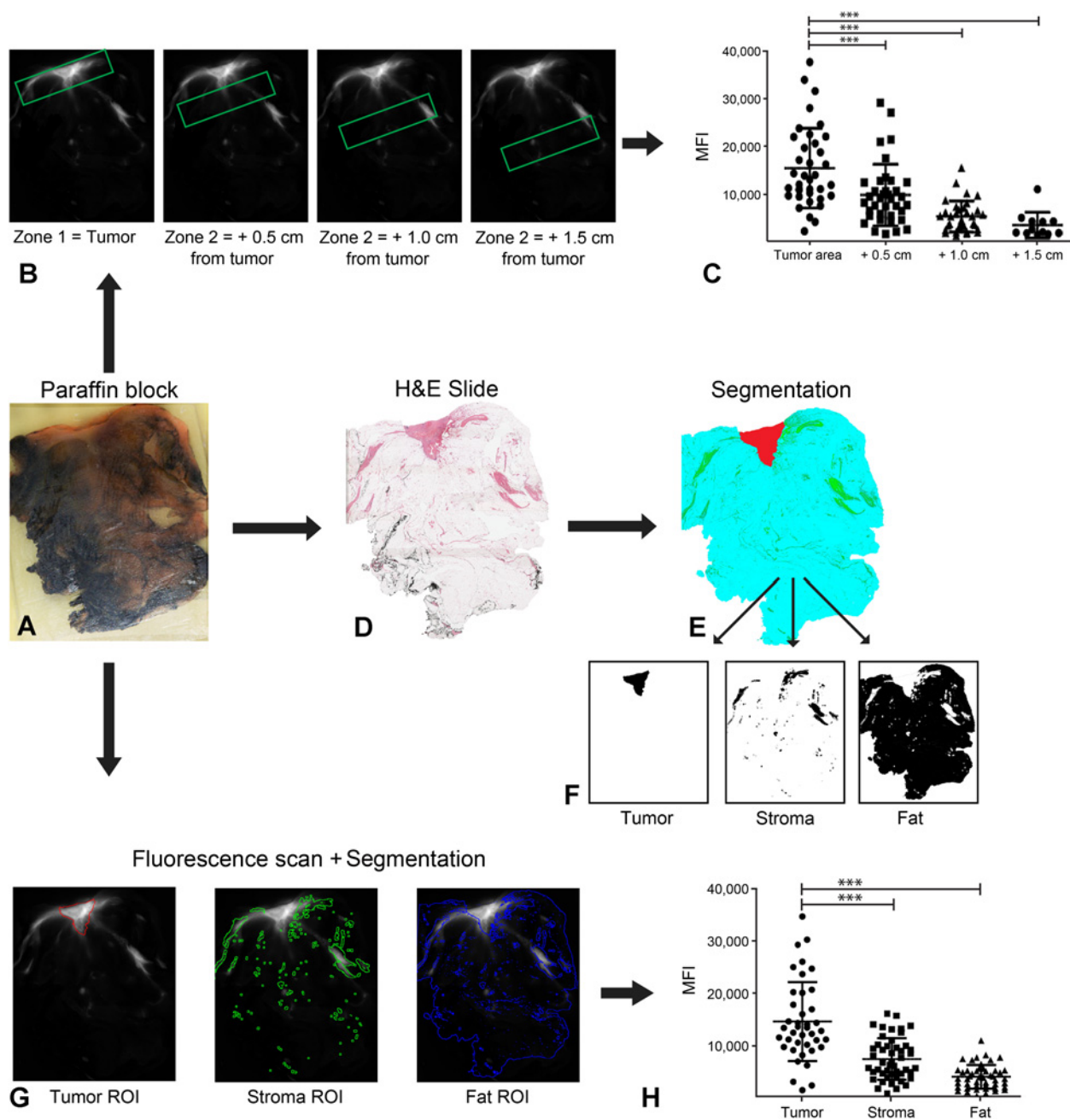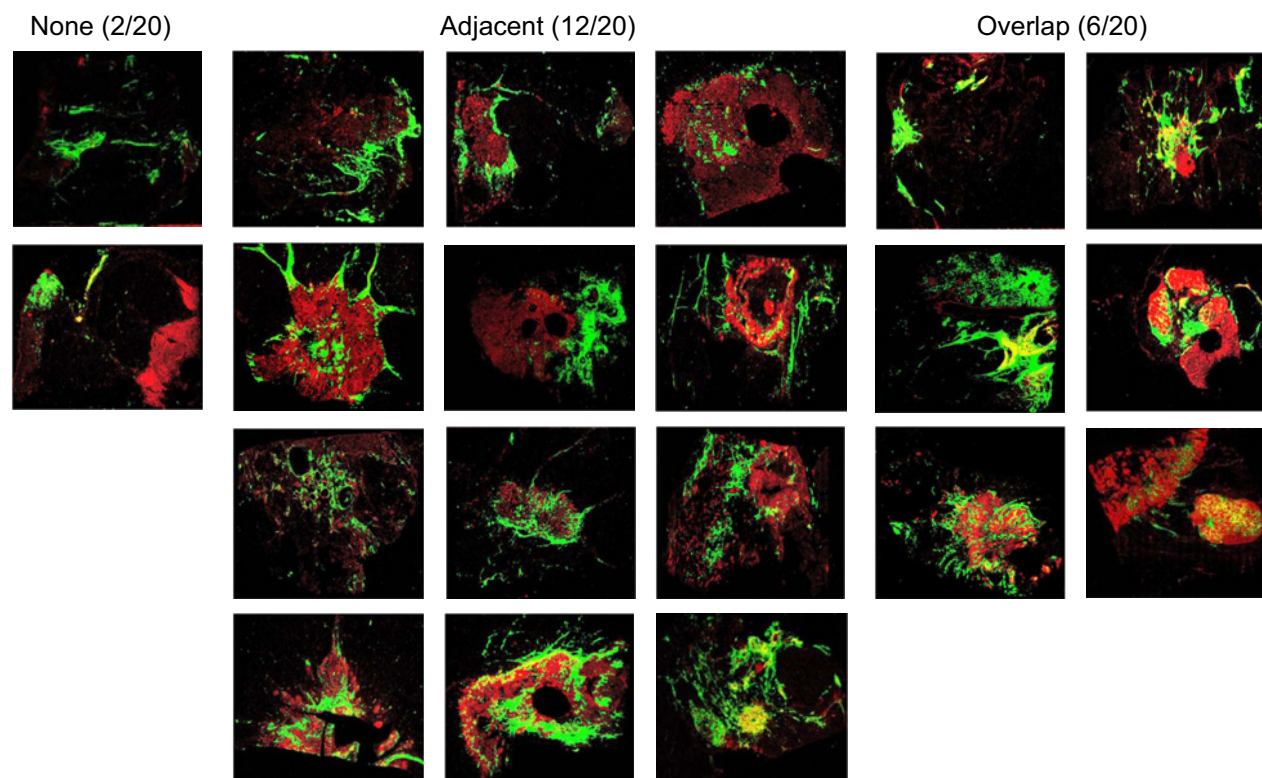
Figure 4.

Macroscopic fluorescence tumor margin assessment. Paraffin blocks were inked for margin assessment as standard of care and subsequently imaged by macroscopic fluorescence imaging, followed by H&E staining (**A**). By defining four tumor margin zones distant from the tumor (i.e., tumor area, 0.5, 1.0, and 1.5 cm, **B**), the MFI was calculated (**C**). MFI of the tumor site was higher than in the tumor margin zones (***, $P < 0.0001$). Macroscopic segmentation of fluorescence tissue localization. Paraffin blocks were scanned (**A**), stained for H&E (**D**), and subsequently segmented (**E** and **F**). For each tissue type, the region of interest (ROI) was delineated [**G,** Tumor (red), stroma (green), and fat (blue)]. Per ROI, MFI was calculated and compared (**F**). Tumor tissue had a higher MFI compared with stroma and fat (**H**; ***, $P < 0.001$).

IRDye800CW was safe with sufficient tumor-specific tracer uptake for margin assessment in primary breast cancer tissue. A novel framework of systematic *ex vivo* macroscopic imaging and fluorescent image analyses of excised specimen, fresh tissue slices, paraffin blocks, and tissue slides showed tumor-specific tracer uptake, thus clearly distinguishing the tumor margins within normal healthy breast tissue. This framework provides a novel tool for evaluation and validation of fluorescent tracers in image-guided surgery. NIR light has low tissue absorption characteristics, mainly caused by hemoglobin, and low autofluorescence properties compared with fluorescent dyes in the visible light (27). In BCS, a negative microscopic resection margin is of great value to

Figure 5.
Colocalization of VEGF-A and bevacizumab–IRDye800CW. Color deconvolution (DAB color layers were converted to red-black images) of immunohistochemical staining for VEGF expression is depicted in red. Near-infrared fluorescence of bevacizumab–IRDye800CW is depicted in green. Between VEGF-A and bevacizumab–IRDye800CW localization, there was in 90% of the patients adjacent/complete overlap (18/20 patients) and no overlap in 10% of the patients (2/20 patients).

reduce a reoperation or the risk of recurrent disease (35), even after adjuvant radiotherapy. An NIRF tumor-specific tracer is therefore the most suitable in terms of sensitivity and specificity whether or not residual tissue (microscopic) is present and should accordingly be excised.

Most prior optical imaging efforts in patients with breast cancer used the nontargeted NIRF tracer ICG, which binds to plasma proteins. This has been tested extensively for lymphatic mapping in breast cancer (36–40). In patients with breast cancer, ICG had SLN identification rates comparable with standard-of-care radiotracers and blue dyes (40). However, ICG is unsuitable due to the limiting formulation and quenching characteristics of the dye for simple and straightforward conjugation to targeting moieties, like antibodies, nanobodies, or small peptides. This precludes its use for tumor-specific targeting by NIRF imaging, as in this study. At this point, two clinical landmark studies have been published on the use of fluorescent targeted antibodies: one study targeting CEA in colorectal cancer (25), and more recently EGFR in head and neck cancer (29). Several approaches have been used showcasing the potential of fluorescence imaging in humans, varying from single-dose to dose-escalation designs differing from our microdosing approach. In particular, the *ex vivo* validation steps for visualization of tumor microdistribution of the NIR fluorescent tracer and its relationship to histologic immunohistochemical parameters provides a framework that was not reported earlier in previous clinical studies in, for example, fluorescein-conjugated

CEA-targeted imaging in colorectal cancer (25), folate receptor-α imaging in ovarian cancer (26), the study of Rosenthal and colleagues using cetuximab–IRDye800CW in head and neck cancer (29), and a protease-activatable probe in soft tissue sarcoma and breast cancer (30). Therefore, the impact of our study is that it provides the necessary framework of evaluation and reporting of future clinical studies of fluorescence image-guided surgery. The *in vivo* targeting characteristics of a GMP fluorescent tracer by applying as a first step the microdosing concept, and thus a low risk of potential adverse events, deliver data on the targeting characteristics of the tracer and subsequently the format for *ex vivo* analyses. If such a study provides the data for tumor-specific targeting, then a subsequent dose-finding or diagnostic accuracy study can be carried out with a higher degree of definitive data. As mentioned by Kummar and colleagues (21), "microdosing studies are designed with the objective to establish at the very earliest opportunity—before a large number of patients have been accrued and exposed to potential drug-associated toxicity—whether an agent is targeting its biological marker in a tumor, and consequently whether further clinical development is warranted" and thus allows selection of tracer candidates more likely to be developed successfully, but also helps in determination of the dosing scheme for the subsequent phase II–III clinical studies.

Although *ex vivo* imaging confirmed tumor-specific uptake in our study, the absolute fluorescent signal intensities of the targeted tracer were too low to identify tumor margins *in situ* during

actual surgery, for which several explanations are possible. First, the tracer dose used in this study may have been too low to reach the threshold for detecting tumor-specific signal intraoperatively originating from microscopic irradical tumor margins. Nevertheless, 90% of all patients using microdosing bevacizumab–IRDye800CW showed adjacent or complete overlap with VEGF-A expression measured by IHC. Second, due to the fact that usually surgical incisions in BCS are small, this might imply that insufficient excitation light reaches the surgical cavity or wound bed or vice versa that emitted NIR light originating from the tracer cannot be collected by the optical imaging system. This might be solved by applying a sterile NIR laparoscope or endoscope close within the wound bed. Third, even with a higher dose, improvements in the sensitivity of the camera system, such as correction algorithms and state-of-the-art charge-coupled device chips, may be required for intraoperative detection of bevacizumab–IRDye800CW.

By increasing the tracer dose to still subtherapeutic doses, a signal above the threshold of healthy surrounding autofluorescent signal can be expected, and intraoperative detection of the fluorescent signal in tumor tissue may be feasible. This has recently been shown by Rosenthal and colleagues up to a maximum dose of 62.5 mg/m^2 of intravenously injected cetuximab–IRDye800CW in patients with head and neck cancer (HNSCC) up (29). Similarly, a large clinically proven safe dose range is still available for a bevacizumab NIR tracer. For example, patients treated for colorectal cancer with neoadjuvant bevacizumab being dosed at 10 to 15 mg/kg every 3 weeks undergo surgery around 6 weeks after the last bevacizumab dose to avoid wound healing problems. With a half-life of 20 days, the remaining circulating bevacizumab level is around 160 mg at that time. This would translate into a minimum 180 mg flat bevacizumab dose, to be injected 3 days before surgery, without increased risk of impaired wound healing. In future studies, we therefore suggest a dose escalation starting around 10 mg and increasing up to the potential maximum of 180 mg. The total costs for microdosing and the procedural costs are estimated to be $1,800. As VEGF-A is overexpressed in >70% of all patients with breast cancer eligible for BCS, preselection by applying a ^{89}Zr–bevacizumab PET imaging study seems redundant and imposes in approximately 30% of the patients an increased radiation risk, which does not outweigh the risks associated with an injection of a nonradioactive fluorescent tracer.

In our clinical study, we used the NIR optical imaging system not only during surgery, but also postoperatively during pathologic examination to image the complete excised specimen, after bread-loaf slicing, in paraffin blocks and on tissue slides. These slice images showed a clear fluorescent signal at the site of the tumor in fresh tissue, as confirmed by fluorescence scanning and microscopy. Fluorescence-guided pathology may thereby assist the pathologist in assessing the important tissue parts or for sensitive sampling, such as tumor margin assessment of a mastectomy or lumpectomy specimens. Moreover, during surgery, the pathologist can immediately report to the surgeon whether all tumors have been excised or whether margins show a fluorescent signal, which might indicate the presence of tumor.

By using MAPI, a systemically injected bevacizumab–IRDye800CW fluorescent tracer was cross-correlated with the presence of tumor (using H&E), VEGF-A expression (by IHC and ELISA), collagen, and microvessel density. Next to visualization of other targets with antibodies, smaller fragments like nanobodies targeting specific tumor markers, such as carbonic anhydrase IX, HER2, and CEA, have been developed more recently for imaging solid tumors. This could also be validated by NIR optical imaging (in situ and ex vivo) and MAPI in future translational clinical studies (41–43). Moreover, this study has shown that MAPI can be used ex vivo to cross-correlate the fluorescent-labeled therapeutic drug bevacizumab and its tumor-specific targeting and local tumor distribution in humans by using excised specimens. This can be done with both macroscopic and microscopic imaging. This novel colocalization methodology provides a reproducible platform in drug development and subsequent dose-finding studies at the tissue and cellular level for other antibodies (therapeutic or otherwise), nanobodies, and small peptides as targeting moiety.

As neoangiogenesis is a universal tumor marker, other tumor types may also benefit from fluorescence imaging using bevacizumab–IRDye800CW. For example, HNSCC, colorectal, and esophageal cancer may be suitable for such imaging, as these tumors are located more superficially, leading to higher fluorescence signals and less negative impact on surrounding tissue (i.e. scattering, penetration issues). Currently, three studies are ongoing to determine feasibility of a fluorescent endoscope attached to the camera system after administration of 4.5 mg bevacizumab–IRDye800CW intravenously to detect rectal cancer, esophageal cancer, and premalignant and malignant polyps in familial adenomatous polyposis (ClinicalTrials.gov identifiers NCT01972373, NCT02129933, and NCT02113202). This approach is therefore of interest not only for tumor visualization and characterization in intraoperative surgical guidance, but also for diagnostic purposes, drug development, and treatment monitoring (42).

In conclusion, this is the first clinical study to demonstrate safety and feasibility of the NIR fluorescent tracer bevacizumab–IRDye800CW for tumor-specific optical imaging in patients with primary breast cancer. Probably, because the administered dose (i.e., microdose of 4.5 mg – 26 nmol) was low, in situ intraoperative tumor margin detection was not possible. However, immediate NIR optical imaging of the excised specimen in patients with a positive margin confirmed reliable margin assessment by fluorescence. Therefore, ex vivo imaging was highly feasible and correlated well with VEGF-A quantification and microscopic analyses of the tumor site of targeting. Microscopic analyses did not show a complete overlay of the fluorescent signal and the VEGF-A staining. This is probably because bevacizumab–IRDye800CW targets the soluble and extracellular matrix–bound splice variant 121 of VEGF-A (10, 11), whereas the applied immunohistochemical staining mainly detects intracellular VEGF-A expression. For intraoperative in situ imaging purposes, fluorescent intensity values could be optimized using higher tracer doses that are still well below the therapeutic dosing scheme of bevacizumab, such as recently described for cetuximab–IRDye800CW.

We have therefore initiated a subsequent phase II dose-finding study to determine the optimal dose for intraoperative use in patients with primary breast cancer (www.ClinicalTrials.gov identifier: NCT02583568).

Disclosure of Potential Conflicts of Interest

from SurgVision. V. Ntziachritos reports receiving commercial research grants and other commercial research support from SurgVision. G.M. van Dam is a consultant/advisory board member for and reports receiving commercial research grants from SurgVision. No potential conflicts of interest were disclosed by the other authors.

Authors' Contributions

Conception and design: L.E. Lamberts, A.L.L. Adams, A.G.T. Terwissscha van Scheltinga, C.P. Schröder, E. de Boer, W.P.Th.M. Mali, P.J. van Diest, E.G.E. de Vries, V. Ntziachristos, G.M. van Dam

Development of methodology: M. Koch, J.S. de Jong, A.L.L. Adams, J. Glatz, A.G.T. Terwissscha van Scheltinga, M.N. Lub-de Hooge, E. de Boer, S. Oliveira, P.J. van Diest, E.G.E. de Vries, V. Ntziachristos, G.M. van Dam

Acquisition of data (provided animals, acquired and managed patients, provided facilities, etc.): L.E. Lamberts, M. Koch, J.S. de Jong, A.L.L. Adams, J. Glatz, M.E.G. Kranendonk, A.G.T. Terwissscha van Scheltinga, L. Jansen, J. de Vries, M.N. Lub-de Hooge, C.P. Schröder, E. de Boer, B. van der Vegt, S. Oliveira, A.J. Witkamp, W.P.Th.M. Mali, E. Van der Wall, P.J. van Diest, E.G.E. de Vries, G.M. van Dam

Analysis and interpretation of data (e.g., statistical analysis, biostatistics, computational analysis): M. Koch, J.S. de Jong, A.L.L. Adams, J. Glatz,

M.E.G. Kranendonk, A.G.T. Terwissscha van Scheltinga, J. de Vries, B. van der Vegt, W.B. Nagengast, S.G. Elias, P.J. van Diest, E.G.E. de Vries, G.M. van Dam

Writing, review, and/or revision of the manuscript: L.E. Lamberts, M. Koch, J.S. de Jong, A.L.L. Adams, J. Glatz, M.E.G. Kranendonk, A.G.T. Terwissscha van Scheltinga, L. Jansen, J. de Vries, M.N. Lub-de Hooge, C.P. Schröder, A. Jorritsma-Smit, M.D. Linssen, E. de Boer, B. van der Vegt, W.B. Nagengast, S.G. Elias, S. Oliveira, A.J. Witkamp, E. Van der Wall, P.J. van Diest, E.G.E. de Vries, G.M. van Dam

Administrative, technical, or material support (i.e., reporting or organizing data, constructing databases): L.E. Lamberts, J.S. de Jong, A.L.L. Adams, M.E.G. Kranendonk, A. Jorritsma-Smit, M.D. Linssen, E. de Boer

Study supervision: C.P. Schröder, S.G. Elias, W.P.Th.M. Mali, P.J. van Diest, E.G.E. de Vries, V. Ntziachristos, G.M. van Dam

Grant Support

References

1. International Agency for Research on Cancer. GLOBOCAN: World cancer statistics. Lyon, France: International Agency for Research on Cancer; 2012.
2. Waljee JF, Hu ES, Newman LA, Alderman AK. Predictors of re-excision among women undergoing breast-conserving surgery for cancer. Ann Surg Oncol 2008;15:1297–303.
3. Biglia N, Maggiorotto F, Liberale V, Bounous VW, Sqro LG, Pecchio S, et al. Clinical-pathologic features, long term-outcome and surgical treatment in a large series of patients with invasive lobular carcinoma (ILC) and invasive ductal carcinoma (IDC). Eur J Surg Oncol 2013;39:455–60.
4. Park CC, Mitsumori M, Nixon A, Recht A, Connolly J, Gelman R, et al. Outcome at 8 years after breast-conserving surgery and radiation therapy for invasive breast cancer: Influence of margin status and systemic therapy on local recurrence. J Clin Oncol 2000;18:1668–75.
5. Chagpar AB, Martin RC, Hagendoorn LJ, Chao C, McMasters KM. Lumpectomy margins are affected by tumor size and histologic subtype but not by biopsy technique. Am J Surg 2004;188:399–402.
6. Pleijhuis RG, Graafland M, de Vries J, Bart J, de Jong JS, van Dam GM. Obtaining adequate surgical margins in breast-conserving therapy for patients with early-stage breast cancer: current modalities and future directions. Ann Surg Oncol 2009;16:2717–30.
7. Ferrara N, Davis-Smyth T. The biology of vascular endothelial growth factor. Endocr Rev 1997;18:4–25.
8. Amini A, Masoumi Moghaddam S, Morris DL, Pourgholami MH. The critical role of vascular endothelial growth factor in tumor angiogenesis. Curr Cancer Drug Targets 2012;12:23–43.
9. Liu Y, Tamimi RM, Collins LC, Schnitt SJ, Gilmore HL, Connolly JL, et al. The association between vascular endothelial growth factor expression in invasive breast cancer and survival varies with intrinsic subtypes and use of adjuvant systemic therapy: results from the Nurses' Health Study. Breast Cancer Res Treat 2011;129:175–84.
10. Viacava P, Naccarato AG, Bocci G, Fanelli G, Aretini G, Lonobile A, et al. Angiogenesis and VEGF expression in pre-invasive lesions of the human breast. J Pathol 2004;204:140–6.
11. Nagengast WB, Hooge MN, van Straten EM, Kruijff S, Brouwers AH, den Dunnen WF, et al. VEGF-SPECT with 111In-bevacizumab in stage III/IV melanoma patients. Eur J Cancer 2011;47:1595–602.
12. Slamon DJ, Godolphin W, Jones LA, Holt JA, Wong SG, Keith DE, et al. Studies of the HER-2/neu proto-oncogene in human breast and ovarian cancer. Science 1989;244:707–12.
13. Slamon D, Eiermann W, Robert N, Pienkowski T, Martin M, Press M, et al. Adjuvant trastuzumab in HER2-positive breast cancer. New Engl J Med 2011;365:1273–83.
14. Lamberts LE, Williams SP, Terwissscha van Scheltinga AG, Lub-de Hooge MN, Schröder CP, Gietema JA, et al. Antibody positron emission tomog-

raphy imaging in anticancer drug development. J Clin Oncol 2015;33:1491–504.
15. Desar IM, Stillebroer AB, Oosterwijk E, Leenders WP, van Herpen CM, van der Graaf WT, et al. 111In-bevacizumab imaging of renal cell cancer and evaluation of neoadjuvant treatment with the vascular endothelial growth factor receptor inhibitor sorafenib. J Nucl Med 2010;51:1707–15.
16. Scheer MG, Stollman TH, Boerman OC, Verrijp K, Sweep FC, Leenders WP, et al. Imaging liver metastases of colorectal cancer patients with radiolabelled bevacizumab: lack of correlation with VEGF-A expression. Eur J Cancer 2008;44:1835–40.
17. Oosting SF, Brouwers AH, van Es SC, Nagengast WB, Oude Munnink TH, Lub-de Hooge MN, et al. 89Zr-bevacizumab PET visualizes heterogeneous tracer accumulation in tumor lesions of renal cell carcinoma patients and differential effects of antiangiogenic treatment. J Nucl Med 2015;56:63–9.
18. van Asselt SJ, Oosting SF, Brouwers AH, Bongaerts AH, de Jong JR, Lub-de Hooge MN, et al. Everolimus reduces 89Zr-bevacizumab tumor uptake in patients with neuroendocrine tumors. J Nucl Med 2014;55:1087–92.
19. Gaykema SB, Brouwers AH, Lub-de Hooge MN, Pleijhuis RG, Timmer-Bosscha H, Pot L, et al. 89Zr-bevacizumab PET imaging in primary breast cancer. J Nucl Med 2013;54:1014–8.
20. U.S. Food and Drug Administartion. Guidance for Industry, Investigators and Reviewers/Exploratory IND studies, Silver Spring, MD: FDA Center for Drug Evaluation and Research. Available from: http://www.fda.gov/downloads/drugs/guidancecomplianceregulatoryinformation/guidances/ucm078933.pdf.
21. Kummar S, Doroshow JH, Tomaszewski JE, Calvert AH, Lobbezoo M, Giaccone G, et al. Task force on methodology for the development of innovative cancer therapies (MDICT). Phase 0 clinical trials: recommendations from the task force on methodology for the development of innovative cancer therapies. Eur J Cancer 2009;45:741–6.
22. Vokes EE, Salgia R, Karrison TG. Evidence-based role of bevacizumab in non-small cell lung cancer. Ann Oncol 2013;24:6–9.
23. Hurwitz HI, Tebbutt NC, Kabbinavar F, Giantonio BJ, Guan ZZ, Mitchell L, et al. Efficacy and safety of bevacizumab in metastatic colorectal cancer: Pooled analysis from seven randomized controlled trials. Oncologist 2013;18:1004–12.
24. Escudier B, Bellmunt J, Négrier S, Bajetta E, Melichar B, Bracarda S, et al. Phase III trial of bevacizumab plus interferon alfa-2a in patients with metastatic renal cell carcinoma (AVOREN): final analysis of overall survival. J Clin Oncol 2010;28:2144–50.
25. Folli S, Wagnières G, Pèlegrin A, Calmes JM, Braichotte D, Buchegger F, et al. Immunophotodiagnosis of colon carcinomas in patients injected with fluoresceinated chimeric antibodies against carcinoembryonic antigen. Proc Natl Acad Sci U S A 1992;89:7973–7.

26 van Dam GM, Themelis G, Crane LMA, Harlaar NJ, Pleijhuis RG, Kelder W, et al. Intraoperative tumor-specific fluorescence imaging in ovarian cancer by folate receptor-α targeting: First in-human results. Nat Med 2011;17: 1315–9.

27 Frangioni JV. New technologies for human cancer imaging. J Clin Oncol 2008;26:4012–21.

28 Burggraaf J, Kamerling IM, Gordon PB, Schrier L, de Kam ML, Kales AJ, et al. Detection of colorectal polyps in humans using an intravenously administered fluorescent peptide targeted against c-Met. Nat Med 2015;21:955–61.

29 Rosenthal EL, Warram JM, de Boer E, Chung TK, Korb ML, Brandwein-Gensler M, et al. Safety and tumor-specificity of cetuximab-IRDye800 for surgical navigation in head and neck cancer. Clin Cancer Res 2015;21: 3658–66.

30 Whitley MJ, Cardona DM, Lazarides AL, Spasojevic I, Ferrer JM, Cahill J, et al. A mouse-human phase 1co-clinical trial of a protease-activated fluorescent probe for imaging cancer. Sci Transl Med 2016;8:320ra4.

31 Terwisscha van Scheltinga AG, van Dam GM, Nagengast WB, Ntziachristos V, Hollema H, Herek JL, et al. Intraoperative near-infrared fluorescence tumor imaging with vascular endothelial growth factor and human epidermal growth factor receptor 2 targeting antibodies. J Nucl Med 2011;52:1778–85.

32 Ter Weele EJ, Terwisscha van Scheltinga AG, Linssen MD, Nagengast WB, Lindner I, Jorritsma-Smit A, et al. Development, preclinical safety, formulation, and stability of clinical grade bevacizumab-800CW, a new near infrared fluorescent imaging agent for first in human use. Eur J Pharm Biopharm 2016;104:226–34.

33 Richtlijnen Database. Dutch Guidelines for Breast Cancer 2.0. Utrecht, the Netherlands: Knowledge Institute of Medical Specialists. Available from: http://richtlijnendatabase.nl/en/richtlijn/breast_cancer/breast_cancer.html.

34 Oliveira S, Cohen R, Walsum MS, van Dongen GA, Elias SG, van Diest PJ, et al. A novel method to quantify IRDye800CW fluorescent antibody probes

35 ex vivo in tissue distribution studies. Eur J Nucl Med Mol Imaging Res 2012;25:50.

35 Pleijhuis RG, Kwast AB, Jansen L, Vries J, Lanting R, Bart J, et al. A validated web-based nomogram for predicting positive surgical margins following breast-conserving surgery as a predictive tool for clinical decision-making. Breast 2013;22:773–9.

36 Troyan SL, Kianzad V, Gibbs-Strauss SL, Gioux S, Matsui A, Oketokoun R, et al. The FLARE intraoperative near-infrared fluorescence imaging system: A first-in-human clinical trial in breast cancer sentinel lymph node mapping. Ann Surg Oncol 2009;16:2943–52.

37 Murawa D, Hirche C, Dresel S, Hünerbein M. Sentinel lymph node biopsy in breast cancer guided by indocyanine green fluorescence. Br J Surg 2009;96:1289–94.

38 Hojo T, Nagao T, Kikuyama M, Akashi S, Kinoshita K. Evaluation of sentinel node biopsy by combined fluorescent and dye method and lymph flow for breast cancer. Breast 2010;19:210–3.

39 Schaafsma BE, Mieog JS, Hutteman M, van der Vorst JR, Kuppen PJ, Löwik CW, et al. The clinical use of indocyanine green as a near-infrared fluorescent contrast agent for image-guided oncologic surgery. J Surg Oncol 2011;104:323–32.

40 Mieog JS, Troyan SL, Hutteman M, Donohoe KJ, van der Vorst JR, Stockdale A, et al. Toward optimization of imaging system and lymphatic tracer for near-infrared fluorescent sentinel lymph node mapping in breast cancer. Ann Surg Oncol 2011;18:2483–91.

41 Luker GD, Luker KE. Optical imaging: Current applications and future directions. J Nucl Med 2008;49:1–4.

42 de Boer E, Harlaar NJ, Taruttis A, Nagengast WB, Rosenthal EL, Ntziachristos V, et al. Optical innovations in surgery. Br J Surg 2015;102:e56–72.

43 Rosenthal EL, Warram JM, Basilion JP, Biel MA, Bogyo M, Bouvet M, et al. Successful translation of fluorescence navigation during oncologic surgery: a consensus report. J Nucl Med 2015;57:144–50.

Clinical Cancer Research

Tumor-Specific Uptake of Fluorescent Bevacizumab–IRDye800CW Microdosing in Patients with Primary Breast Cancer: A Phase I Feasibility Study

Laetitia E. Lamberts, Maximillian Koch, Johannes S. de Jong, et al.

Updated version	Access the most recent version of this article at: doi:10.1158/1078-0432.CCR-16-0437
Supplementary Material	Access the most recent supplemental material at: http://clincancerres.aacrjournals.org/content/suppl/2016/11/09/1078-0432.CCR-16-0437.DC1

Cited articles	This article cites 40 articles, 15 of which you can access for free at: http://clincancerres.aacrjournals.org/content/23/11/2730.full#ref-list-1

E-mail alerts	Sign up to receive free email-alerts related to this article or journal.
Reprints and Subscriptions	To order reprints of this article or to subscribe to the journal, contact the AACR Publications Department at pubs@aacr.org.
Permissions	To request permission to re-use all or part of this article, use this link http://clincancerres.aacrjournals.org/content/23/11/2730. Click on "Request Permissions" which will take you to the Copyright Clearance Center's (CCC) Rightslink site.